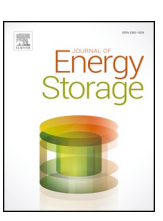
FISEVIER

Contents lists available at ScienceDirect

Journal of Energy Storage

journal homepage: www.elsevier.com/locate/est



Degradation of magnesium-ion battery anodes by galvanic replacement reaction in all-phenyl complex electrolyte



Zeyu Wang^{a,b}, Arkamita Bandyopadhyay^a, Hemant Kumar^a, Manni Li^{a,c}, Akshaya Venkatakrishnan^a, Vivek B. Shenoy^a, Eric Detsi^{a,d,*}

- ^a Department of Materials Science & Engineering, University of Pennsylvania, Philadelphia, PA 19104, USA
- ^b State Key Laboratory of Advanced Welding and Joining, Harbin Institute of Technology, Harbin 150001, China
- ^c School of Materials Science and Engineering, Harbin Institute of Technology, Harbin 150001, China
- ^d Vagelos Institute for Energy Science and Technology (VIEST), Philadelphia, PA 19104, USA

ARTICLE INFO

Keywords: Corrosion Mg-ion battery anode All-phenyl-complex Magnesium stannide Galvanic replacement

ABSTRACT

In this work, experimental and computational methods based on density functional theory (DFT) were used to study the spontaneous degradation (i.e. in the absence of any external electromotive force) of pure metallic magnesium (Mg) and magnesium stannide (Mg₂Sn) in all-phenyl complex (APC) electrolyte, a commonly used Mg-ion battery electrolyte. Our results reveal that Mg atoms can be stripped from metallic Mg and from Mg₂Sn through galvanic replacement reactions involving anions present in APC such as Ph₄Al⁻, Ph₂AlCl₂, PhAlCl₃ and AlCl₄, resulting in Mg dissolution and metallic aluminum deposition. Such a spontaneous degradation phenomenon is susceptible to impact the performance of Mg-ion battery cells in which metallic Mg or magnesium alloys are used as anodes. In particular, we have found that Mg-ion battery half-cells assembled using Mg₂Sn and metallic Mg as the working and counter electrodes, respectively, and APC as the electrolyte, exhibit Coulombic efficiencies higher than 100% at low C-rates. Such an unusual Coulombic efficiency is attributed to unbalance charge associated with the difference in Mg atoms dissolution rate between the Mg₂Sn working electrode and the Mg metal counter electrode, when these electrodes undergo spontaneous degradation in APC.

1. Introduction

Recently Mg-ion batteries (MIBs) have received renewed interest as promising alternative to Li-ion batteries (LIBs), owing to the high availability of raw Mg resources, the divalent nature of Mg²⁺, which can transfer twice as much electrons as monovalent Li⁺, a reduced risk of physical hazards when metallic Mg is exposed to air, and the nondendritic nature of Mg metal [1–4]. Despite these remarkable features, the development of practical MIBs has been hindered by the lack of suitable electrolytes that are compatible with Mg metal [5-8]. Specifically, conventional salts and organic solvent combinations similar to those successfully used in LIBs commonly form a Mg-ion-blocking passivating film onto Mg metal anodes [9-12]. As a consequence, only a few classes of electrolytes are compatible with Mg metal as negative electrode [3,13,22,14-21], among which all-phenyl complex (APC), a second generation organohaloaluminate electrolyte developed by Aurbach et al. [15,23-25]. The APC electrolyte derived from in situ reaction between 2 equivalents of Lewis base phenylmagnesium chloride (PhMgCl) and 1 equivalent of Lewis acid aluminum trichloride (AlCl₃)

in tetrahydrofuran (THF) solvent was designed to improve the oxidative stability beyond ~2.2 V vs. Mg/Mg²⁺ by replacing the Grignard alkyl ligand with phenyl group, which excludes the β-H elimination source [23,24]. Thus, APC is considered to be a suitable MIB electrolyte in the voltage window below ~2.2 V vs. Mg/Mg²⁺, beyond which it becomes corrosive [25-29]. While previous studies on the corrosive nature of APC have focused on the corrosion of current collectors and stainless steel coin cell cases by chloride ion (Cl⁻) at polarization voltages beyond $2.2\,V$ vs. Mg/Mg²⁺ [1,25,28,30,31], the corrosion of Mg metal and its alloys have rarely been studied despite the fact that metallic Mg is more vulnerable to corrosion than the stainless steel coin cell parts previously investigated. It is anticipated that APC-induced degradation of Mg metal and Mg alloys used as anodes in MIBs will negatively impact the cell performance. In the present work, we investigate the spontaneous corrosion (i.e. in the absence of externally applied potential) of Mg metal and Mg alloys in APC electrolyte. We show that anions present in APC such as Ph4Al, Ph2AlCl2, PhAlCl3 and AlCl4 can extract electrons from metallic Mg and Mg alloys, resulting in Mg dissolution and Al metal deposition, a process known as galvanic

^{*} Corresponding author at: Department of Materials Science & Engineering, University of Pennsylvania, Philadelphia, PA 19104, USA. E-mail address: detsi@seas.upenn.edu (E. Detsi).

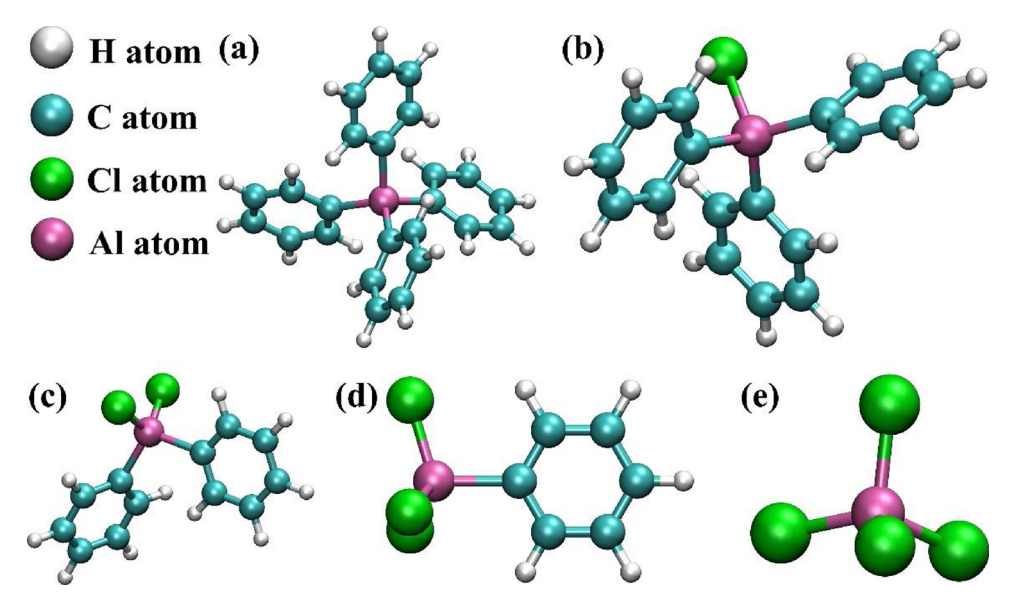


Fig. 1. Optimized geometries of (a) Ph₄Al⁻, (b) Ph₃AlCl⁻, (c) Ph₂AlCl₂⁻, (d) Ph₄AlCl₃⁻ and (e) AlCl₄⁻.

replacement [32]. In the first part of the *Results and Discussion* section, we use density functional theory (DFT) to demonstrate that the above-mentioned anions are indeed susceptible to extract elemental Mg from Mg metal and Mg alloys (e.g. Mg₂Sn) through galvanic replacement reaction. In the second part of the *Results and Discussion* section, we verify experimentally that elemental Mg can spontaneously dissolve from Mg alloy (namely Mg₂Sn) kept in APC. In the third part of the *Results and Discussion* section, we investigate the impact of APC-induced Mg dissolution on the electrochemical performance of MIBs by comparing the Coulombic efficiencies of MIB half-cells cycled in APC at various C-rates.

2. Experimental section

2.1. Chemicals and materials preparation

 $\rm Mg_2Sn$ alloy was fabricated by melting Mg chips (99.98% Sigma-Aldrich) and Sn shot (Sigma-Aldrich, 99.8%). The corresponding alloy ingot was mechanically grinded into powder in an argon-filled glove box, followed by 6 h ball-milling (Spex 8000 mixer/mill machine) to further reduce the particle size as in our previous work [33]. APC electrolyte was made using phenylmagnesium chloride (PhMgCl, 2 M in THF, Sigma-Aldrich), aluminum chloride (AlCl_3, anhydrous, 99.99%, Sigma-Aldrich) and tetrahydrofuran (THF, > 99.9% anhydrous, Sigma-Aldrich) [33].

2.2. Material characterizations

X-ray diffraction (XRD) patterns of the pristine Mg₂Sn and Mg₂Sn samples kept for corrosion in APC electrolyte for 15 and 30 days were acquired using a Rigaku GeigerFlex X-ray diffractometer equipped with a graphite monochromator, and using the K α 1 line of a Cu X-ray tube. All patterns were collected on a Bragg angle range of 30-95° with the steps of 0.05° and a scan rate of 2° min⁻¹. Energy dispersive X-ray spectroscopy (EDX) was carried out using an Oxford Instruments EDX Li-Si drift detector. X-ray photoelectron spectroscopy (XPS) was conducted using a PHI Versaprobe 5000 scanning X-ray photoelectron spectrometer.

2.3. Electrochemical characterization

Mg-ion battery working electrodes were prepared using the ball-milled Mg₂Sn powder. Typically, 50 wt. % of Mg₂Sn powder was mixed

with 30 wt. % of conductive carbon additives (10 wt. % carbon nanofiber, 10 wt. % graphene nanosheets and 10 wt. % carbon black), and 20 wt. % of binder (polyvinylidene fluoride/N-Methyl-2-pyrrolidone -PVDF/NMP) to make a homogeneous slurry, which was then cast onto a copper current collector in an argon-filled glove box. As-cast Mg₂Sn slurry was dried under vacuum for overnight followed by heating in the argon glove box at 200 °C for 1 h for further drying. After drying, working electrode samples with active material (Mg₂Sn) loading of 1.0–2.0 mg cm $^{-2}$ were punch-cut and assembled into 2032 type coin cells with Mg foil as the counter and reference electrode, binder-free glass microfiber as the separator, and 0.4 M APC electrolyte. (De) magnesiation tests were performed using a Bio-Logic VMP-300 potentiostat.

2.4. Computational methods

Structural optimization of APC anions, metallic Mg and Mg₂Sn were performed using DFT with the hybrid B3LYP exchange-correlation functional as implemented in GAMESS suite of packages [34]. A 6-311++G (d,p) Gaussian basis set was employed for all the optimization and electronic property calculations. An implicit solvent method was used: Polarizable Continuum Model (PCM) using the integral equation formalism variant (IEFPCM) [35], where THF is considered as solvent as indicated by this experiment and previous theoretical studies [32].

3. Results and discussion

3.1. Spontaneous dissolution of Mg in APC studied by density functional theory

Density functional calculations were performed to study the effect of APC electrolyte on metallic Mg and Mg alloy (Mg₂Sn). All the possible anions (Ph_nAlCl_{4-n}) (n = 0–4) in the APC electrolyte were modeled as depicted in Fig. 1. To model the materials (Mg and Mg₂Sn), we considered bulk 3D structures of Mg and Mg₂Sn. As GAMESS considers molecular systems, we took a 48 atoms bulk supercell without the periodic boundary condition as a cluster to mimic bulk materials (it should not be confused with metallic cluster purely, as we have preserved the bulk Mg/Mg₂Sn optimized geometry throughout the calculation). The ionization energies of the two materials were calculated by taking out an electron from them to model the reaction between APC and bulk materials in uncharged state. Our calculation shows the

Table 1 HOMO (H) - LUMO (L) energies and ΔG_{red} values for the anions in the APC electrolyte.

System	H (eV)	L (eV)	ΔG_{red} (eV)
Ph ₄ Al ⁻	-5.63	-0.07	0.24
Ph ₃ AlCl ⁻	-5.87	-0.11	0.344
Ph ₂ AlCl ₂ ⁻	-6.02	-0.15	0.55
PhAlCl ₃ ⁻	-6.43	-0.25	0.64
AlCl ₄ ⁻	-7.46	-0.67	0.994

presence of net Mulliken charges of zero and +0.13 e on Mg atoms from metallic Mg and Mg₂Sn samples, respectively. Although Mg₂Sn is formed by a stannide anion and a Mg cation, due to the covalent nature of the compound it does not show full positive charge on Mg atoms. This confirms the electron donating probability of Mg atoms in both systems. When we consider a +1 charged state of the systems, we find that the energy needed to donate an electron by these systems is 1.81 eV for Mg and 2.53 eV for Mg₂Sn, suggesting an easier electron transfer process from metallic Mg to APC anions. Also, the Mg⁺¹/Mg⁰ electrode potential with respect to standard hydrogen electrode (SHE) is found to be -2.63 V vs SHE, which compares well with -2.7 V vs SHE in reported literature data [36].

Next, we considered the APC electrolyte and calculate the HOMO and LUMO energies as well as changes in Gibbs Free Energy of solvation associated with the reduction of the APC electrolyte molecules (ΔG_{red}). The LUMO energy determines the ease of electron acceptance in the system. The values are summarized in Table 1. We found that the HOMO and LUMO energies compare well with literature data [29]. We also calculated for Mg metal the Mg_{sol}^{+1}/Mg_{bulk} and Mg_{sol}^{+2}/Mg_{bulk} potentials and found them to be -0.13 and -0.32 eV, respectively. The HOMO (H) - LUMO (L) energies and ΔG_{red} values of the APC electrolyte suggest that all the APC anions can donate electrons to Mg electrode if it is involved in a stepwise one-electron transfer process, and all the APC anions except PhAl₄ can donate electrons in a twoelectron transfer pathway. For Mg₂Sn, we also calculated the Mg_{sol}/ Mg_{Mg2Sn} and Mg_{sol}^{+2}/Mg_{Mg2Sn} potentials and found them to be -0.15 and -0.43 eV, respectively, making two-electron transfer not possible for both Ph₄Al and Ph₃AlCl. Thus, the reaction in APC electrolyte can involve one- or two-electron transfer pathway. Moreover, our results suggest that the formation of Mg2+ ions and Al metal in the reaction medium may occur easier for Mg metal than for Mg₂Sn. The stabilization energies of the reacting systems are included in Table S1.

3.2. Spontaneous dissolution of Mg from Mg_2Sn in APC

The ball-milled Mg₂Sn powder was kept in 0.4 M APC in an argonfilled glove box for several days in order to investigate the corrosive effect of APC. The crystal structure and chemical composition of Mg₂Sn was investigated after 15 and 30 days corrosion in APC (Mg₂Sn-15 and Mg₂Sn-30 for abbreviations, respectively), and compared with the crystal structure of pristine Mg₂Sn that has not been exposed to APC. Fig. 2 shows the XRD patterns of pristine Mg₂Sn, Mg₂Sn-15 and Mg₂Sn-30. The blue pattern labeled (i) in Fig. 2 corresponds to the XRD pattern of the pristine material; prior to exposure to APC the starting Mg₂Sn is composed of cubic Mg₂Sn (PDF#86-2265). The XRD data of Mg₂Sn-15 alloy exhibits both cubic Mg₂Sn diffraction peaks (PDF#86-2265) and β-Sn diffraction peaks (PDF#86-2264) as shown by the red XRD pattern labeled (ii) in Fig. 2a and b. The emergence of the β-Sn peaks indicates that elemental Mg has been removed from Mg₂Sn under the influence of APC, resulting in the exposure of metallic Sn. The black XRD pattern labeled (iii) corresponds to the Mg₂Sn-30 sample, which also reveals β-

The chemical compositions of the pristine Mg_2Sn , Mg_2Sn -15 and Mg_2Sn -30 samples were qualitatively and quantitatively investigated by energy dispersive X-ray spectroscopy (EDX). Results are shown in

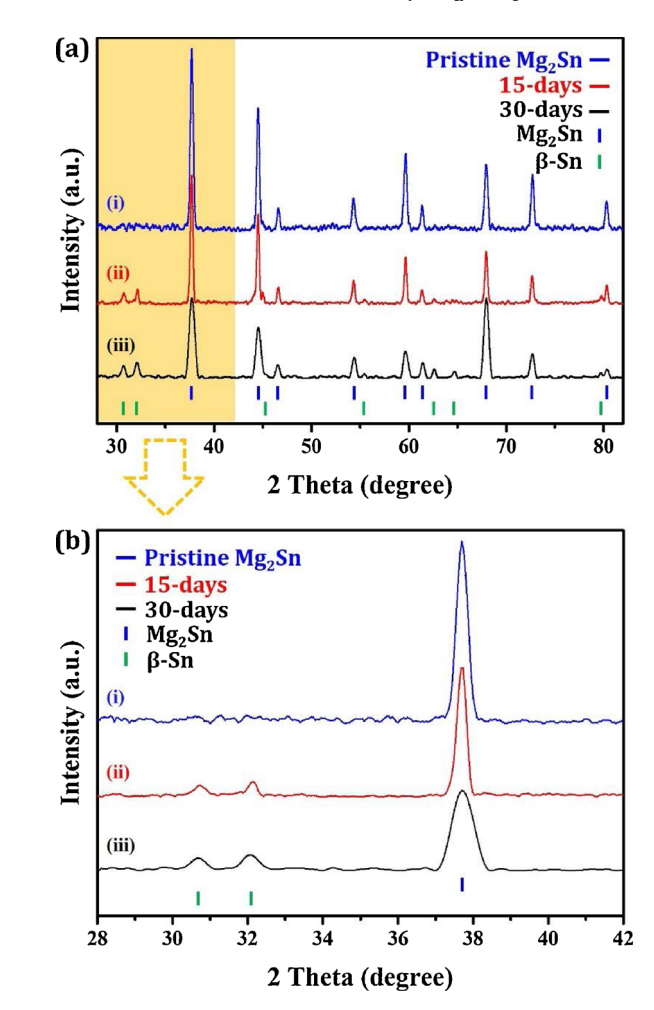


Fig. 2. XRD patterns of pristine Mg_2Sn (blue), Mg_2Sn -15 (red) and Mg_2Sn -30 (black) samples. (a) Full spectra; (b) Selected spectra to illustrate the appearance of β-Sn diffraction peaks after exposure to APC (For interpretation of the references to colour in this figure legend, the reader is referred to the web version of this article).

Fig. 3a, b and c for the pristine Mg₂Sn, Mg₂Sn-15 and Mg₂Sn-30 samples, respectively; and in Table 2. Qualitatively, the most noticeable difference between the three samples is the appearance of Al signal on the EDX spectra of the Mg₂Sn-15 and Mg₂Sn-30. Quantitatively, the EDX results show a gradual decrease in the Mg content relative to Sn from a Mg-to-Sn atomic ratio of ~60:40 in the pristine sample down to ~52:45 in the Mg₂Sn-15 sample and ~47:49 in the Mg₂Sn-30 sample. These data clearly suggest that a significant fraction of Mg atoms has been removed from the starting Mg₂Sn, in agreement with computational prediction in the previous section. Our DFT results also predict that elemental Mg can dissolve spontaneously from metallic Mg in APC. Note that in the present experimental section, we have only verified the dissolution of elemental Mg from Mg₂Sn (not from pure Mg) in APC because it is more practical to track the relative amount of Mg dissolved in APC (in our case the ratio between Mg and Sn), instead of tracking the absolute amount of Mg removed in the case of pure metallic Mg. Based on our DFT data, Mg removal from Mg2Sn occurred through galvanic replacement reaction between Al-based anions present in APC and elemental Mg from Mg₂Sn. Such a galvanic replacement process results in the deposition of metallic Al, which may explain the appearance of Al signal from the EDX spectra of the Mg₂Sn-15 and Mg₂Sn-30 samples.

Since the APC electrolyte is made from $AlCl_3$, even though APC-corroded Mg_2Sn samples have been thoroughly rinsed in pure THF prior to EDX characterization, it can be argued that Al signals from our EDX

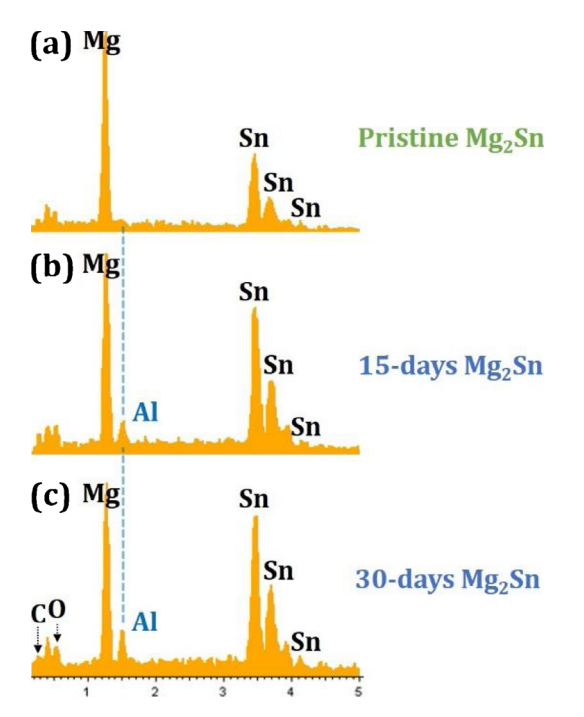


Fig. 3. EDX spectra of the (a) pristine Mg_2Sn , (b) Mg_2Sn-15 (c) Mg_2Sn-30 samples.

Table 2 Chemical compositions of (a) pristine Mg_2Sn alloy, (b) Mg_2Sn -15 and (c) Mg_2Sn -30 samples.

Element	Pristine Mg ₂ Sn	Mg ₂ Sn-15	Mg ₂ Sn-30
Mg	~ 60	~ 52	~ 47
Al	0	~ 3	~ 4
Sn	~ 40	~ 45	~ 49

spectra come from residual APC electrolyte on these samples. Therefore, the APC-corroded samples were further investigated by Xray photoelectron spectroscopy (XPS) to determine the oxidation state of Al. The XPS survey spectra of the samples are shown in Fig. S1. The deconvoluted Al 2p core level spectra from the pristine Mg₂Sn and Mg₂Sn-30 are shown in Fig. 4a and b, respectively. While no trace of metallic Al was observed from the pristine Mg₂Sn (Fig. 4a), metallic Al, as well as Al from Al₂O₃ and Al from Al-Cl were detected in the Mg₂Sn-30 sample (Fig. 4b) [37–39]. While the presence of Al from Al-Cl can be attributed to residual Al-based species from the APC electrolyte, the presence of metallic Al and Al₂O₃ cannot be associated with residual APC electrolyte [32]. Instead, metallic Al most likely comes from the reduction of Al-containing anions to Al⁰. In addition, the presence of Al from Al₂O₃ can be attributed to the oxidation of some Al⁰ during sample exposure in air for material characterization. Fig. 4c and d depict the deconvoluted O 1s core level XPS spectrum in the pristine Mg₂Sn and the 30-day exposed Mg₂Sn, respectively. For the pristine Mg₂Sn (Fig. 4c), O in MgO, SnO and SnO2 have been detected [40-42]. The simultaneous presence of Sn^{2+} and Sn^{4+} has been observed by other groups [40,43]. After 30 days of corrosion, the peak of O in Al₂O₃ appeared, matching well with the peak of Al in Al₂O₃, as shown in Fig. 4d [44]. This further confirms that Al was formed during corrosion. The experimental results above confirm that Mg dissolves from Mg₂Sn in APC by galvanic replacement as schematized in Fig. 5, in agreement with our DFT calculations. Previous studies on the corrosion behavior of APC have mainly focused on chloride cation as potential corroding agent at relatively high polarization potentials (> 2.2 V vs Mg), as mentioned earlier in our introduction [25,26,31]. APC is an in-situ generated inorganic electrolyte containing THF-coordinated Mg complex including $(Mg_2(\mu\text{-Cl})_3\cdot 6THF)^+$ cations, and Al-containing inorganic species such as $(AlCl_n^4-Ph_n)^-$ (n=0–4) anions [2,15,25,45]. The present work shows these anions can corrode metallic Mg and Mg alloys in the absence of any external polarization potential. The presence of these species in APC electrolyte has been confirmed by Pour et al. [32] who suggested the following reaction during the preparation of APC from 2 equivalents of PhMgCl Lewis base and 1 equivalent of AlCl $_3$ Lewis acid in THF solvent:

$$PhMgCl + 4.5 AlCl_3 \rightarrow Ph_4Al^{-} + 2 Ph_2AlCl_2 + PhAlCl_3 + 0.5 AlCl_4 + 4.5 Mg_2Cl_3^{+}$$
 (1)

Our DFT calculation results predict favorable reactions between these Al-based anions and Mg from Mg metal and Mg alloys (Mg₂Sn), in agreement with our experimental results on the spontaneous dissolution of elemental Mg from Mg₂Sn in APC. The dissolution of elemental Mg by Al-based anions has also been reported in the case of AlCl₄ through the following galvanic replacement reaction during which Al metal is deposited [46,47]:

$$AlCl_4 + 6Mg + 6THF \rightarrow 4Al + 3[Mg_2(\mu-Cl)_3\cdot6THF]^+ + 7Cl_- (2)$$

Al deposition as in Eq. (2) is consistent with our EDX and XPS results for the Mg_2Sn-15 and Mg_2Sn-30 samples. An interesting question corresponds to the impact of APC-induced corrosion on the performance of MIB cells using Mg metal as negative or as counter electrode. This point is addressed in the next section.

3.3. Impact of APC-induced Mg dissolution on the performance of MIB cells

MIB half-cells using APC as the electrolyte were investigated in coin cell configurations with Mg₂Sn as the working electrode and Mg metal as the counter and reference electrodes [33]. XRD and electron microscopy data demonstrating the reversible (de)magnesiation of Mg₂Sn in this half-cell configuration was recently reported in our previous work [33]. Typical electrochemical data obtained during (de)magnesiation of Mg₂Sn at various C-rates are shown in Fig. 6. The first (de) magnesiation cycle of Mg₂Sn at the rates of 1 C (red), C/2 (blue), C/5 (green), C/10 (light blue) and C/50 (grey) are shown in Fig. 6a. At each of these C-rates, the demagnesiation capacity is clearly higher than the magnesiation capacity. This implies that the Coulombic efficiency (defined here as "100 x magnesiation capacity over demagnesiation capacity") is less than 100% during the all the 1st cycles, as illustrated by the black makers in Fig. 6c. These Coulombic efficiencies below 100% (black markers in Fig. 6c) are normal since fundamentally, faradaic charge transfer processes are quasi-reversible or irreversible, meaning that Coulombic efficiencies should be less than 100%. Besides the charge transfer irreversibility, pulverization of the active materials during the first demagnesiation step results in dead materials (i.e. active materials that are no longer electrically connected to the current collector, and hence become electrochemically inactive) in the electrode [33]. Dead materials formed during the first demagnesiation step hinder a full charge recovery during subsequent magnesiation steps. Hence, Coulombic efficiencies less than 100% should be expected at all C-rates during cycling. Interestingly, on the contrary of the 1st cycles where Coulombic efficiencies are less than 100% irrespective of the Crate, during the 2nd and 3rd cycles, the demagnesiation and re-magnesiation capacities are comparable at high C-rates (1 C and C/2), but at low C-rates (C/5, C/10 and C/50) the demagnesiation capacity is clearly lower than the re-magnesiation capacity as shown in Fig. 6b. Consequently, at these low C-rates, Coulombic efficiencies are higher than 100% during the 2nd (red markers in Fig. 6c) and 3rd (blue markers in Fig. 6c) cycles. For example, at C/10, the first magnesiation capacity is ~310 mA h g⁻¹ compared to ~400 mA h g⁻¹ for the first demagnesiation capacity (see light blue curve in Fig. 6a). However, during cycling at C/10, this magnesiation capacity increases from ~310 mA h g $^$ in the 1st cycle to ~380 mAh g⁻¹ in the 3rd cycle, while the

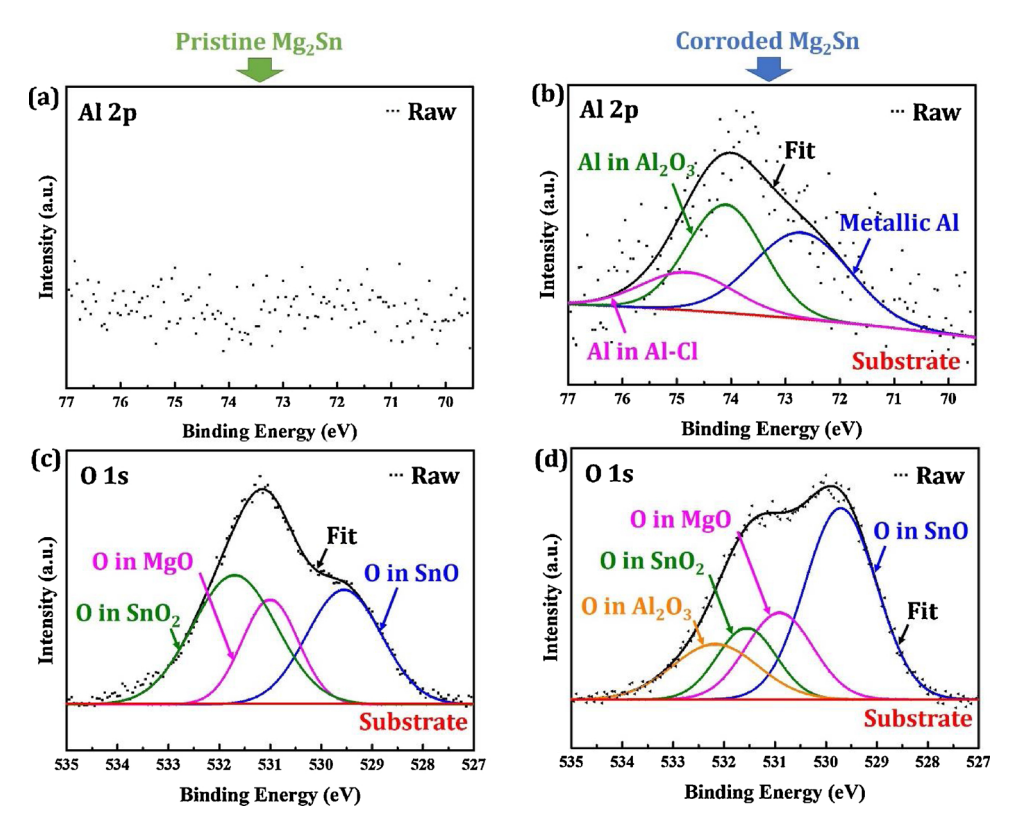


Fig. 4. (a, b) Deconvoluted Al 2p and (c, d) deconvoluted O 1s core level XPS spectrum of (a, c) pristine Mg₂Sn alloy and (b, d) Mg₂Sn-30 samples.

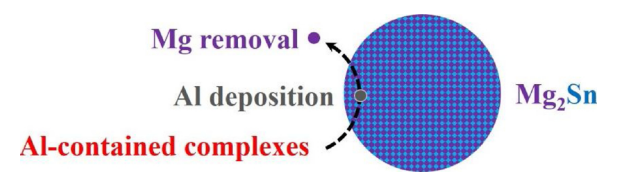


Fig. 5. Mechanism of Mg dissolution from Mg_2Sn by galvanic replacement reaction in APC.

demagnesiation capacity decreases from ~400 mA h g $^{-1}$ in the first cycle to ~320 mA h g $^{-1}$ in the 3rd cycle (see light blue curve in Fig. 6b). The decrease in the magnesiation capacity from ~400 mA h g $^{-1}$ (1st cycle) to ~320 mA h g $^{-1}$ (3rd cycle) is expected and can be rationalized by materials failure as mentioned above. Since the demagnesiation capacity decreases in subsequent cycles (i.e. after the 1st cycle), one also expects the re-magnesiation capacity to decrease. However, this is not the case because the re-magnesiation capacity increases during subsequent cycles as stated above. The increase in the re-magnesiation capacity from ~310 mA h g $^{-1}$ (1st cycle) to ~380 mA h g $^{-1}$ (3rd cycle) is unexpected and gives rise to Coulombic efficiencies higher than 100%

at low C-rates after the first cycle. This seems to violate thermodynamics rules since Coulombic efficiencies higher than 100% will mean that more Mg is electrochemically stripped from the Mg metal counter electrode and store in the Mg₂Sn working electrode (i.e. magnesiation of the working electrode) than the amount of Mg electrochemically removed from the Mg₂Sn working electrode and plated onto the Mg metal counter electrode (demagnesiation of the working electrode). The most likely explanation of Coulombic efficiencies beyond 100% is the "spontaneous" dissolution of Mg from the Mg metal counter electrode and from the Mg₂Sn working electrode by galvanic replacement reaction, in addition to Mg dissolution through electrochemical stripping during (de)magnesiation. Based on the above experimental results on Mg₂Sn exposure to APC, the spontaneous dissolution of Mg from Mg₂Sn is a relatively slow process. Similarly, the spontaneous dissolution of pure Mg metal in APC is expected to be relatively slow, which suggests that the longer Mg metal and Mg2Sn are exposed to APC, the more they will dissolve. Interestingly, in the case of our MIB half-cells, at lower C-rates during which the Mg metal counter electrode and the Mg₂Sn working electrode are exposed for longer times to APC, the Coulombic efficiencies are clearly higher than 100%, while at high

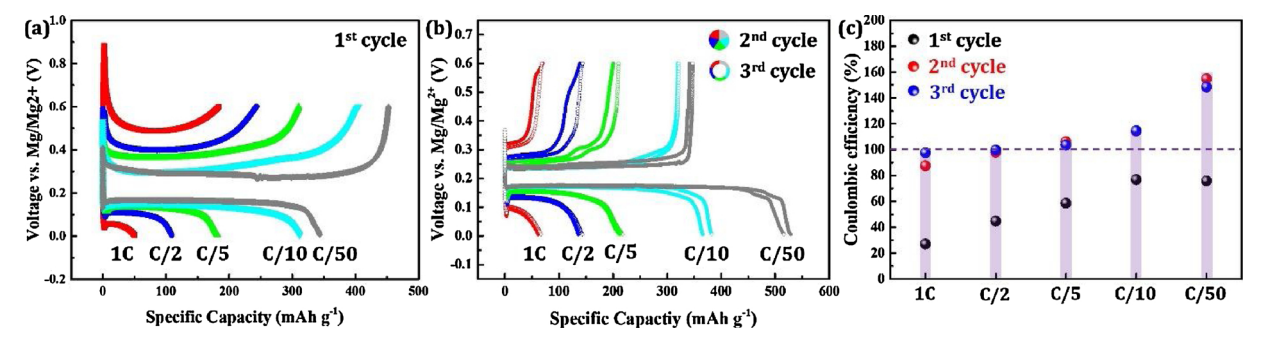


Fig. 6. Electrochemical performance of Mg₂Sn working electrode. Demagnesiation and magnesiation capacities at various C-rates for the (a) 1st cycle, the (b) 2nd and 3rd cycles; (c) Coulombic efficiencies for the 1st, 2nd and 3rd cycles at various C-rates.

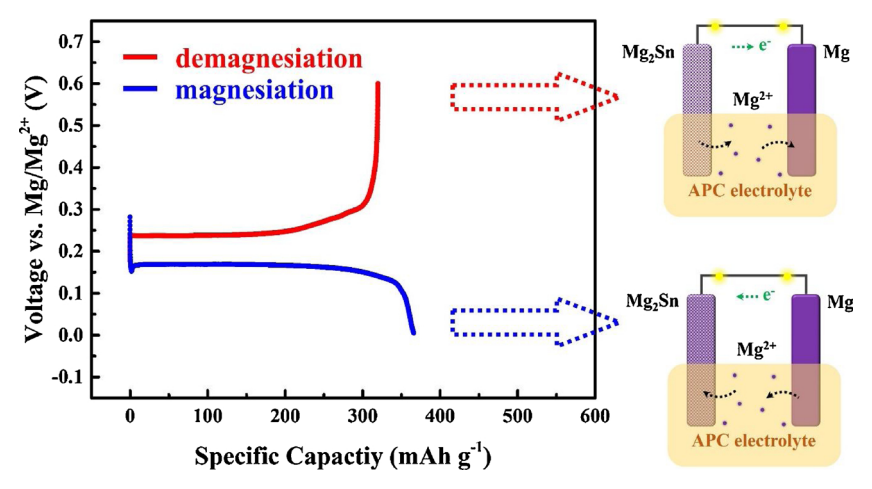


Fig. 7. Schematic of the (de)magnesiation process.

C-rates during which the Mg and Mg₂Sn exposure to APC is limited, the Coulombic efficiencies only approach 100%. This suggests that the cell performance is affected by the spontaneous corrosion of the Mg and Mg₂Sn electrodes in APC. The process can be rationalized as follows (see Fig. 7): during subsequent demagnesiation cycles (2nd, 3rd, etc...), a positive current is used to remove Mg from the Mg2Sn working electrode and deposit it onto the Mg metal counter electrode, resulting in the red galvanostatic curve in Fig. 7 (see also the corresponding graphical electrodes reactions as given by the dashed red arrow). Since the sign of current (positive) is such that the reduction of Mg²⁺ takes place on the counter electrode (i.e. Mg is plated onto the Mg metal counter electrode), this step does not favor the spontaneous oxidation of the Mg metal counter electrode (i.e. the spontaneous dissolution of Mg from the Mg metal counter electrode is not favorable). In the meantime, during this demagnesiation step, Mg will be removed from the Mg₂Sn working electrode electrochemically (i.e. applied positive current) and also spontaneously through galvanic replacement as reported above. The counter reaction for this spontaneous reaction is Al deposition on the Mg₂Sn working electrode as illustrated graphically in Fig. 5.

Also, during subsequent (2nd, 3rd, etc) re-magnesiation cycles, a negative current is now used to remove Mg from the Mg metal counter electrode and store it into the Mg₂Sn working electrode, resulting in the blue galvanostatic curve in Fig. 7 (see also the corresponding graphical electrodes reactions as given by the dashed blue arrow). Since the sign of current (negative) is such that Mg is introduced in the Mg_2Sn working electrode, the reduction of Mg²⁺ takes place on the working electrode. This step does not favor the spontaneous dissolution of Mg₂Sn working electrode. In the meantime, during this re-magnesiation step, Mg is stripped from the Mg metal counter electrode electrochemically (applied negative current) and also spontaneously through galvanic replacement. The counter reaction for this spontaneous reaction is Al deposition on the Mg metal counter electrode as illustrated graphically in Fig. 5 in the case of Mg₂Sn. Thus, both the Mg₂Sn working electrode and the Mg metal counter electrode undergo spontaneous dissolution by galvanic replacement. Based on our DFT results, the spontaneous dissolution of Mg from Mg metal is more favorable than from Mg₂Sn. Hence, during a full cycle (i.e demagnesiation and remagnesiation), there is net unbalance charge associated with Mg metal dissolution. This may justify why after the 1st cycle the Coulombic efficiencies are higher than 100% at low C-rates.

4. Conclusion

In summary, APC-induced spontaneous degradation of metallic Mg and Mg₂Sn was studied using DFT calculations in combination with *ex situ* XRD, EDX and XPS characterizations. It was found that anions present in APC including $(Ph_nAlCl_{4-n})^{-}$ (n = 0–4) can extract electrons

from metal Mg and Mg₂Sn, resulting in the dissolution of elemental Mg from these materials and deposition of metallic aluminum, a process known as galvanic replacement reaction. The electrochemical performance of Mg-ion battery half-cells using APC as the electrolyte, Mg₂Sn as the working electrode and metallic Mg as the counter and reference electrodes was scrutinized in terms of Coulombic efficiency and unusual Coulombic efficiencies higher than 100% were observed at low C-rates. Such Coulombic efficiencies were rationalized by unbalanced charge associated with the difference in APC-induced Mg dissolution rate between the Mg₂Sn working electrode and Mg counter electrode. These results suggest that the spontaneous degradation of Mg-ion battery electrodes in APC impacts the performance of Mg-ion battery cells when Mg or magnesium alloys are used as the anode.

Acknowledgements

The authors are thankful to Penn Engineering and NSF for the financial supports through the PI startup and the NSF-EAGER program with Award number: CMMI-1840672. This work was also carried out in part at the Singh Center for Nanotechnology, part of the National Nanotechnology Coordinated Infrastructure Program, which is supported by the NSF grant NNCI-1542153.

Appendix A. Supplementary data

Supplementary material related to this article can be found, in the online version, at doi:https://doi.org/10.1016/j.est.2019.02.022.

References

- J. Muldoon, C.B. Bucur, T. Gregory, Fervent hype behind magnesium batteries: an open call to synthetic chemists—electrolytes and cathodes needed, Angew. Chemie Int. Ed. 56 (2017) 12064–12084, https://doi.org/10.1002/anie.201700673.
- [2] L. Wang, B. Jiang, P.E. Vullum, A.M. Svensson, A. Erbe, S.M. Selbach, H. Xu, F. Vullum-Bruer, High interfacial charge storage capability of carbonaceous cathodes for Mg batteries, ACS Nano 12 (2018) 2998–3009, https://doi.org/10.1021/acsnano.8b00753.
- [3] Z. Zhang, Z. Cui, L. Qiao, J. Guan, H. Xu, X. Wang, P. Hu, H. Du, S. Li, X. Zhou, S. Dong, Z. Liu, G. Cui, L. Chen, Novel design concepts of efficient Mg-Ion electrolytes toward high-performance magnesium-selenium and magnesium-sulfur batteries, Adv. Energy Mater. 7 (2017), https://doi.org/10.1002/aenm.201602055.
- [4] H.S. Kim, T.S. Arthur, G.D. Allred, J. Zajicek, J.G. Newman, A.E. Rodnyansky, A.G. Oliver, W.C. Boggess, J. Muldoon, Structure and compatibility of a magnesium electrolyte with a sulphur cathode, Nat. Commun. 2 (2011) 427, https://doi.org/ 10.1038/ncomms1435.
- [5] D. Aurbach, Z. Lu, A. Schechter, Y. Gofer, H. Gizbar, R. Turgeman, Y. Cohen, M. Moshkovich, E. Levi, Prototype systems for rechargeable magnesium batteries, Nature 407 (2000) 724–727, https://doi.org/10.1038/35037553.
- [6] Y. Gofer, N. Pour, D. Aurbach, Electrolytic solutions for rechargeable magnesium batteries, lithium batter, Adv. Technol. Appl. (2013) 327–347, https://doi.org/10. 1002/9781118615515.ch15.
- [7] H.D. Yoo, I. Shterenberg, Y. Gofer, G. Gershinsky, N. Pour, D. Aurbach, Mg

- rechargeable batteries: an on-going challenge, Energy Environ. Sci. 6 (2013) 2265–2279, https://doi.org/10.1039/c3ee40871j.
- [8] D. Aurbach, I. Weissman, Y. Gofer, E. Levi, Nonaqueous magnesium electrochemistry and its application in secondary batteries, Chem. Rec. 3 (2003) 61–73, https://doi.org/10.1002/tcr.10051.
- [9] Z. Lu, A. Schechter, M. Moshkovich, D. Aurbach, On the electrochemical behavior of magnesium electrodes in polar aprotic electrolyte solutions, J. Electroanal. Chem. 466 (1999) 203–217, https://doi.org/10.1016/S0022-0728(99)00146-1.
- [10] O. Tutusaus, R. Mohtadi, N. Singh, T.S. Arthur, F. Mizuno, Study of electrochemical phenomena observed at the Mg metal/electrolyte interface, ACS Energy Lett. 2 (2017) 224–229, https://doi.org/10.1021/acsenergylett.6b00549.
- [11] O.R. Brown, R. McIntyre, The magnesium and magnesium amalgam electrodes in aprotic organic solvents a kinetic study, Electrochim. Acta 30 (1985) 627–633, https://doi.org/10.1016/0013-4686(85)80104-3.
- [12] D. Aurbach, N. Pour, 13 Non-aqueous electrochemistry of magnesium (Mg), Corros. Magnes. Alloy (2011) 484–515, https://doi.org/10.1533/9780857091413.
- [13] D. Aurbach, A. Schechter, M. Moshkovich, Y. Cohen, On the mechanisms of reversible magnesium deposition processes, J. Electrochem. Soc. 148 (2001) A1004–A1014, https://doi.org/10.1149/1.1387980.
- [14] D. Aurbach, Magnesium deposition and dissolution processes in ethereal grignard salt solutions using simultaneous EQCM-EIS and in situ FTIR spectroscopy, Electrochem. Solid-State Lett. 3 (1999) 31, https://doi.org/10.1149/1.1390949.
- [15] O. Mizrahi, N. Amir, E. Pollak, O. Chusid, V. Marks, H. Gottlieb, L. Larush, E. Zinigrad, D. Aurbach, Electrolyte solutions with a wide electrochemical window for rechargeable magnesium batteries, J. Electrochem. Soc. 155 (2008) A103, https://doi.org/10.1149/1.2806175.
- [16] R. Mohtadi, M. Matsui, T.S. Arthur, S.J. Hwang, Magnesium borohydride: from hydrogen storage to magnesium battery, Angew. Chemie Int. Ed. 51 (2012) 9780–9783, https://doi.org/10.1002/anie.201204913.
- [17] Z. Zhang, S. Dong, Z. Cui, A. Du, G. Li, G. Cui, Rechargeable magnesium batteries using conversion-type cathodes: a perspective and minireview, Small Methods 2 (2018) 1800020, https://doi.org/10.1002/smtd.201800020.
- [18] A. Du, Z. Zhang, H. Qu, Z. Cui, L. Qiao, L. Wang, J. Chai, T. Lu, S. Dong, T. Dong, H. Xu, X. Zhou, G. Cui, An efficient organic magnesium borate-based electrolyte with non-nucleophilic characteristics for magnesium-sulfur battery, Energy Environ. Sci. 10 (2017) 2616–2625, https://doi.org/10.1039/C7EE02304A.
- [19] N. Singh, T.S. Arthur, C. Ling, M. Matsui, F. Mizuno, A high energy-density tin anode for rechargeable magnesium-ion batteries, Chem. Commun. (Camb). 49 (2013) 149–151, https://doi.org/10.1039/c2cc34673g.
- [20] L.R. Parent, Y. Cheng, P.V. Sushko, Y. Shao, J. Liu, C.M. Wang, N.D. Browning, Realizing the full potential of insertion anodes for Mg-ion batteries through the nanostructuring of Sn, Nano Lett. 15 (2015) 1177–1182, https://doi.org/10.1021/ nl5042534.
- [21] O.I. Malyi, T.L. Tan, S. Manzhos, In search of high performance anode materials for Mg batteries: computational studies of Mg in Ge, Si, and Sn, J. Power Sources 233 (2013) 341–345, https://doi.org/10.1016/j.jpowsour.2013.01.114.
- [22] Z. Wang, Q. Su, J. Shi, H. Deng, G.Q. Yin, J. Guan, M.P. Wu, Y.L. Zhou, H.L. Lou, Y.Q. Fu, Comparison of tetragonal and cubic tin as anode for Mg Ion batteries, ACS Appl. Mater. Interfaces 6 (2014) 6786–6789, https://doi.org/10.1021/am500554y.
- [23] R. Mohtadi, F. Mizuno, Magnesium batteries: current state of the art, issues and future perspectives, Beilstein J. Nanotechnol. 5 (2014) 1291–1311, https://doi.org/ 10.3762/binano.5.143
- [24] D. Aurbach, G.S. Suresh, E. Levi, A. Mitelman, O. Mizrahi, O. Chusid, M. Brunelli, Progress in rechargeable magnesium battery technology, Adv. Mater. 19 (2007) 4260–4267. https://doi.org/10.1002/adma.200701495.
- [25] J. Muldoon, C.B. Bucur, A.G. Oliver, J. Zajicek, G.D. Allred, W.C. Boggess, Corrosion of magnesium electrolytes: chlorides – the culprit, Energy Environ. Sci. 6 (2013) 482–487, https://doi.org/10.1039/C2EE23686A.
- [26] A.L. Lipson, S.-D. Han, B. Pan, K.A. See, A.A. Gewirth, C. Liao, J.T. Vaughey, B.J. Ingram, Practical stability limits of magnesium electrolytes, J. Electrochem. Soc. 163 (2016) A2253–A2257, https://doi.org/10.1149/2.0451610jes.
- [27] N. Wu, Z.Z. Yang, H.R. Yao, Y.X. Yin, L. Gu, Y.G. Guo, Improving the electrochemical performance of the $\rm Li_4Ti_5O_{12}$ electrode in a rechargeable magnesium battery by lithium-magnesium co-intercalation, Angew. Chemie Int. Ed. 54 (2015) 5757–5761, https://doi.org/10.1002/anie.201501005.
- [28] S. Yagi, A. Tanaka, Y. Ichikawa, T. Ichitsubo, E. Matsubara, Electrochemical stability of magnesium battery current collectors in a grignard reagent-based electrolyte, J. Electrochem. Soc. 160 (2013) C83–C88, https://doi.org/10.1149/2.

033303ies

- [29] J. Muldoon, C.B. Bucur, A.G. Oliver, T. Sugimoto, M. Matsui, H.S. Kim, G.D. Allred, J. Zajicek, Y. Kotani, Electrolyte roadblocks to a magnesium rechargeable battery, Energy Environ. Sci. 5 (2012) 5941, https://doi.org/10.1039/c2ee03029b.
- [30] I. Bösing, J. Thöming, M. Baune, Electrolyte composition for distinguishing corrosion mechanisms in steel alloy screening, Int. J. Corros. 2017 (2017), https://doi.org/10.1155/2017/9425864.
- [31] E.G. Nelson, S.I. Brody, J.W. Kampf, B.M. Bartlett, A magnesium tetraphenylaluminate battery electrolyte exhibits a wide electrochemical potential window and reduces stainless steel corrosion, J. Mater. Chem. A 2 (2014) 18194–18198, https://doi.org/10.1039/C4TA04625K.
- [32] N. Pour, Y. Gofer, D.T. Major, D. Aurbach, Structural analysis of electrolyte solutions for rechargeable Mg batteries by stereoscopic means and DFT calculations, J. Am. Chem. Soc. 133 (2011) 6270–6278, https://doi.org/10.1021/ja1098512.
- [33] H. Yaghoobnejad Asl, J. Fu, H. Kumar, S.S. Welborn, V.B. Shenoy, E. Detsi, In situ dealloying of bulk Mg2Sn in Mg-Ion half cell as an effective route to nanostructured Sn for high performance Mg-Ion battery anodes, Chem. Mater. (2018), https://doi. org/10.1021/acs.chemmater.7b04124 acs.chemmater.7b04124.
- [34] M.W. Schmidt, K.K. Baldridge, J.A. Boatz, S.T. Elbert, M.S. Gordon, J.H. Jensen, S. Koseki, N. Matsunaga, K.A. Nguyen, S. Su, T.L. Windus, M. Dupuis, J.A. Montgomery, General atomic and molecular electronic structure system, J. Comput. Chem. (1993), https://doi.org/10.1002/jcc.540141112.
- [35] S. Miertuš, E. Scrocco, J. Tomasi, Electrostatic interaction of a solute with a continuum. A direct utilizaion of AB initio molecular potentials for the prevision of solvent effects, Chem. Phys. 55 (1981) 117–129, https://doi.org/10.1016/0301-0104(81)85090-2.
- [36] M.L. Williams, CRC handbook of chemistry and physics, 76th edition, Occup. Environ. Med. 53 (1996), https://doi.org/10.1136/oem.53.7.504 504-504.
- [37] L. Li, Y. Zhang, J. Lei, J. He, R. Lv, N. Li, F. Pan, Water-only hydrothermal method: a generalized route for environmentally-benign and cost-effective construction of superhydrophilic surfaces with biomimetic micronanostructures on metals and alloys, Chem. Commun. 50 (2014) 7416–7419, https://doi.org/10.1039/ c4cc00012a.
- [38] Y. Xiang, C. Zhou, E. Jia, W. Wang, Oxidation precursor dependence of atomic layer deposited Al₂O₃ films in a-Si:H(i)/Al₂O₃ surface passivation stacks, Nanoscale Res. Lett. 10 (2015) 137, https://doi.org/10.1186/s11671-015-0798-2.
- [39] G.E. Mcguire, G.K. Schweitzer, T.A. Carlson, Study of core electron binding energies in some group IIIa, vb, and VIb compounds, Inorg. Chem. 12 (1973) 2450–2453, https://doi.org/10.1021/ic50128a045.
- [40] D.-T. Nguyen, S.-W. Song, Magnesium stannide as a high-capacity anode for magnesium-ion batteries, J. Power Sources 368 (2017) 11–17, https://doi.org/10.1016/j.jpowsour.2017.09.054.
- [41] J. Ma, G. Yang, M. Qin, X. Zheng, H. Lei, C. Chen, Z. Chen, Y. Guo, H. Han, X. Zhao, G. Fang, MgO nanoparticle modified anode for highly efficient SnO₂-Based planar perovskite solar cells, Adv. Sci. 4 (2017) 1700031, https://doi.org/10.1002/advs.201700031.
- [42] D. Shuttleworth, Preparation of metal-polymer dispersions by plasma techniques. An ESCA investigation, J. Phys. Chem. 84 (1980) 1629–1634, https://doi.org/10.1021/i100449a038.
- [43] G. Gaggiotti, A. Galdikas, S. Kačiulis, G. Mattogno, A. Šetkus, Surface chemistry of tin oxide based gas sensors, J. Appl. Phys. 76 (1994) 4467–4471, https://doi.org/ 10.1063/1.357277.
- [44] I. Matolínová, S. Nemšák, M. Cabala, N. Tsud, J. Poltierová-Vejpravová, K. Veltruská, M. Yoshitake, V. Matolín, Growth of Al₂O₃ nanowires on the Cu-9 at. %Al(111) single crystal surface, J. Am. Ceram. Soc. 94 (2011) 4084–4088, https://doi.org/10.1111/j.1551-2916.2011.04704.x.
- [45] J.H. Ha, B. Adams, J.H. Cho, V. Duffort, J.H. Kim, K.Y. Chung, B.W. Cho, L.F. Nazar, S.H. Oh, A conditioning-free magnesium chloride complex electrolyte for rechargeable magnesium batteries, J. Mater. Chem. A (2016), https://doi.org/10. 1039/c6ta01684g.
- [46] K.A. See, K.W. Chapman, L. Zhu, K.M. Wiaderek, O.J. Borkiewicz, C.J. Barile, P.J. Chupas, A.A. Gewirth, The interplay of Al and Mg speciation in advanced Mg battery electrolyte solutions, J. Am. Chem. Soc. 138 (2016) 328–337, https://doi. org/10.1021/jacs.5b10987.
- [47] K.A. See, Y.M. Liu, Y. Ha, C.J. Barile, A.A. Gewirth, Effect of concentration on the electrochemistry and speciation of the magnesium aluminum chloride complex electrolyte solution, ACS Appl. Mater. Interfaces 9 (2017) 35729–35739, https:// doi.org/10.1021/acsami.7b08088.